Scanning Electron Microscopy

Volume 1986
Number 1 *Part I*

Article 8

2-4-1986

Deconvolution in Auger Electron Spectroscopy

B. Chornik
Universidad Simon Bolivar

H. E. Bishop
AERE Harwell

A. Le Moel
CEA-CEN Saclay

C. Le Gressus
CEA-CEN Saclay

SCANNING ELECTRON MICROSCOPY/1986/I (Pages 77-88)
SEM Inc., AMF O'Hare (Chicago), IL 60666-0507 USA

0586-5581/86$1.00+05

DECONVOLUTION IN AUGER ELECTRON SPECTROSCOPY

B. Chornik*, H.E. Bishop°, A. Le Moel, C. Le Gressus

DPC/SSS, CEA-CEN Saclay, 91191 Gif sur Yvette Cedex, France

*Present address: Departamento Ciencia Materiales, Universidad Simon Bolivar, Apartado 80659, Caracas 1080-A, Venezuela

°Present address: Materials Development Div., AERE Harwell, Oxfordshire, OX11 ORA, United Kingdom

(Received for publication March 24, 1984, and in revised form February 04, 1986)

Abstract

Deconvolution calculations have been applied in Auger Electron Spectroscopy to increase resolution and/or to eliminate loss features. We present: i) A short review of the methodology; ii) Recent results obtained in our laboratory in spectroscopy of Al, Ni, Cu, Ag and Te; iii) A discussion on the conditions for the appearance of artefacts originating either in the calculation or the physical processes (emission anisotropy, distribution of electron path lengths, and intrinsic losses).

KEY WORDS: Auger Electron Spectroscopy (AES); Deconvolution; Fast Fourier Transform; Van Cittert iteration; Intrinsic plasmon losses; surface plasmon.

* Address for Correspondence:
Departamento Ciencia Materiales, Universidad Simon Bolivar, Apartado 80659, Caracas 1080-A, Venezuela. Phone Nº (02)962-1301 ext. 8179.

Introduction

Electron energy spectra of solid samples reveal not only the Auger effect,but also additional effects due to energy loss processes and band structure properties. Also there is some broadening due to the finite resolution of the spectrometer. In all cases, each Auger peak is accompanied by a tail at the low energy side, and sometimes characteristic energy loss peaks appear, caused by plasmon generation, interband transitions or core level excitations. Both the energy losses and the instrumental broadening can be described by an integral equation of the convolution type:

$$g(E) = \int_0^\infty f(E')\, h(E-E')\, dE' \qquad (1)$$

where E is the electron kinetic energy, g(E) is the measured spectrum, f(E) is the pure Auger spectrum, and h(E) is the unit response function of the system, which involves energy loss processes and instrumental broadening. Obviously, if h(E) were known, it would be possible to obtain the pure Auger spectrum f(E) by solving the convolution equation. Mularie and Peria (1971) proposed to record the backscattered electron spectrum when the sample is excited by monoenergetic electrons of kinetic energy in the range of the desired Auger spectrum, and to use this measured spectrum as the unit response function of the system. It has been pointed out that this approach is only an approximation (Matthew and Underhill, 1978; Houston, 1975; Tagle et al., 1978, Baro and Tagle, 1978; Madden, 1983; Ramaker et al., 1979) since the backscattering geometry is different to the Auger emission geometry.

Solving the convolution equation for f(E) is a procedure called "deconvolution". In principle, it is possible by this calculation to remove the inelastic tail from each peak, thereby simplifying Auger spectra, and also it is possible to increase resolution. Several surface scientists have used a deconvolution calculation as an intermediate step in data reduction in studies of electronic density of states (Houston, 1975; Tagle et al., 1978; Baro and Tagle, 1978; Madden, 1983; Madden et al., 1978) or molecular structure (Jennison, 1980; Hutson et al., 1982; Campbell et al., 1980; Kelber et al., 1982). A comprehensive review has been published recently by Carley and Joyner (1979), including photoelectron spectroscopy.

LIST OF SYMBOLS

E, E'	Electron kinetic energy.
g(E)	Measured electron spectrum.
f(E)	Intrinsic electron spectrum.
h(E)	Unit response function of the system (including analyser resolution and energy losses).
s	Length of electron path inside the sample.
I_n	Intensity of satellite corresponding to excitation of n volume plasmons.
T(s)	Normalised distribution of electron path lengths.
λ_p	Mean free path for volume plasmon generation.
λ_o	Mean free path for ionisation and other excitation not including plasmons.
λ_{in}	Inelastic mean free path.
λ_l	Elastic transport mean free path.

Our paper presents the results obtained as part of a programme of evaluation of deconvolution, with the aim of applying it to quantitative Auger spectroscopy and to bond identification. Measured Auger spectra and calculated deconvolutions are shown for Al, Ni, Cu, Ag and Te, followed by a discussion of the results, in the light of simple models for plasmon generation and elastic scattering.

Experimental

Most of this work was carried out in a V.G. Escalab MKII spectrometer, which is fitted with a concentric hemispherical analyser (CHA). It was operated in the constant retard ratio mode at 0.12% nominal resolution and the detected signal was direct electron counting. Additional measurements for tellurium were made in a Varian spectrometer with a cylindrical mirror analyser (CMA), energy modulation and lock-in amplifier to obtain first-derivative spectra which were integrated numerically. The CMA has 0.3% nominal resolution.

Samples of Ag, Cu, Ni and Al were mechanically polished; Te samples were cleaved in air. The spectrometer's ultra-high vacuum chamber reached a residual pressure in the 10^{-10} Torr range. Each sample was cleaned by argon ion bombardment and subsequently annealed, checking that oxygen and carbon Auger peaks were not detectable.

Computation Methodology

Having tried several types of deconvolution calculation we chose a development of the Van Cittert iteration as this proved most convenient to program. In order to speed up convergence, an over-relaxation factor is introduced as suggested by Jansson (1970). Each iteration involves a calculation of a convolution between the unit response function and the previous iteration result. We perform this step very quickly by means of a Fast Fourier Transform algorithm (FFT). Since this algorithm assumes implicitly that the functions are periodic, it is necessary to take special precautions to avoid errors. In our case, we doubled the length of each spectrum with added zeroes. This is the easiest implementation of the methods proposed by Helms (1967) which deal with the problem of periodicity in convolution calculations. It has been demonstrated (Madden and Houston, 1976) that in some cases the iteration method may introduce artefacts. This is due to the fact that after a finite number of iterations, the resulting spectrum is a smoothed version of the exact deconvolution (Wertheim, 1975), but the corresponding effective filter in Fourier space may be too sharp, so that Gibbs oscillations may appear in the deconvoluted spectrum. We eliminated this problem by iterating a great number of times (for example, 50 to 100 times) and then applying a filter which does not produce noticeable Gibbs oscillations. Since we are using FFT for the convolution step, it is advantageous to filter in Fourier space with a Blackmann-Harris window (Harris, 1978), which is very similar to the Blackmann window already proposed and used with good success by Tagle et al. (1978). Smoothing in Fourier space or in energy space is mandatory, since deconvolution enhances noise (Jones and Misell, 1970). This scheme of iterating 50 to 100 times is only feasible because we use a very fast algorithm for the convolution step (as described above). The total number of iterations was not critical. We watched a CRT display of successive iterated spectra and decided to stop when we saw no appreciable change. Noise starts to build up at the beginning (say after 6 to 10 iterations) and later the relevant spectrum is completely buried in noise; this fact does not imply that the calculation diverges. The spectrum is recovered at the end with the low-pass filter calculation, which eliminates the high- frequency components of the noise.

A background subtraction was calculated before each deconvolution. We fitted a straight line to the high energy side of each spectrum by means of a standard least squares method. We assumed that this extrapolated straight line was the background, and subtracted it accordingly. This approximation was found to be acceptable for present purposes but a more sophisticated approach would be required for lower energy peaks where there is an appreciable curvature of the background.

Results

Aluminium: The spectra presented in figure 1 are from a single crystal, with a polished (111) face oriented so that the 10 kV primary beam was at (or near) a $|110|$ direction. In spite of the fact that strong variations of KLL Auger intensities were observed as a function of orientation (Bishop et al., 1984), no noticeable changes on the relative intensities of different loss peaks were apparent on the deconvoluted spectra. A polycrystalline aluminium sample produced results (not shown) which were essentially identical to those of figure 1. The peaks at 1376.5 eV and 1361 eV are the first and second volume plasmons from the $KL_{2,3}L_{2,3}(^1D)$ Auger peak at 1392 eV. Although the second plasmon is almost entirely removed by the deconvolution procedure there is still a substantial contribution from the first plasmon in the deconvoluted spectrum.

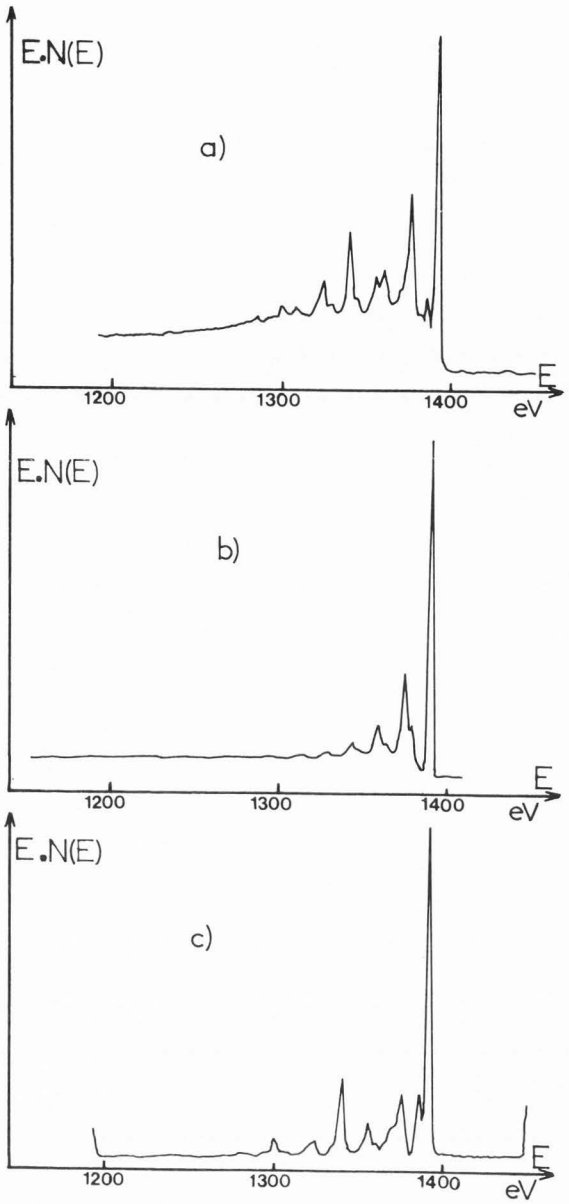

Fig. 1 Aluminium single crystal, (111) face.
1024 channels, 0.25 eV per channel.
a) KLL Auger spectrum
b) Backscattered electron energy spectrum
c) Deconvolution.

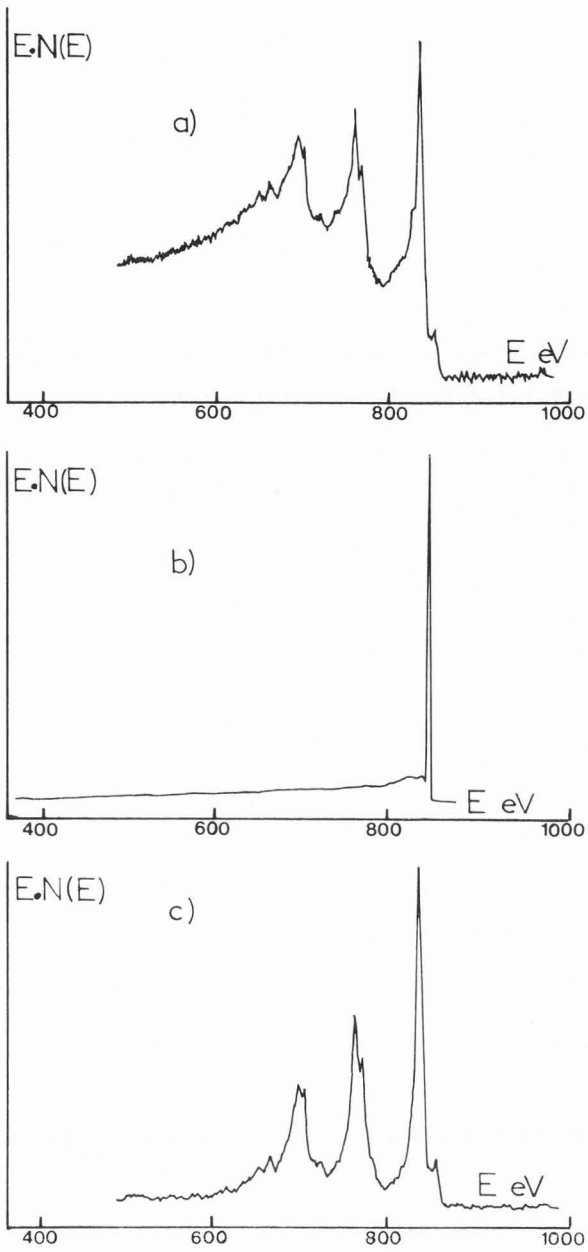

Fig. 2 Polycrystalline nickel.
1024 channels, 0.5 eV per channel
a) LMM Auger spectrum
b) Backscattered electron energy spectrum
c) Deconvolution.

Nickel and copper: LMM spectra of polycrystalline samples are shown in figures 2 and 3 (note that the energy scale is different in both). The deconvolution removes the observed loss features quite efficiently, however a small residual tail remains at the low energies probably the result of a non-linear component in the background.

Silver : A $M_{4,5}N_{4,5}N_{4,5}$ spectrum of polycrystalline sample is shown in figure 4. Note that there is a broad negative lobe at the low energy side of the main Auger peak.

Tellurium: Spectra are shown in figures 5 to 9; the exposed cleaved surfaces are $(1\bar{1}00)$. The main peaks are $M_{4,5}N_{4,5}N_{4,5}$ Auger transitions. Deconvolutions with the corresponding elastic peak spectrum again produce a lobe at the low energy side of the main Auger peak, located at the volume plasmon energy. In order to study this feature, spectra were taken at different orientations of the sample with respect to the primary beam and

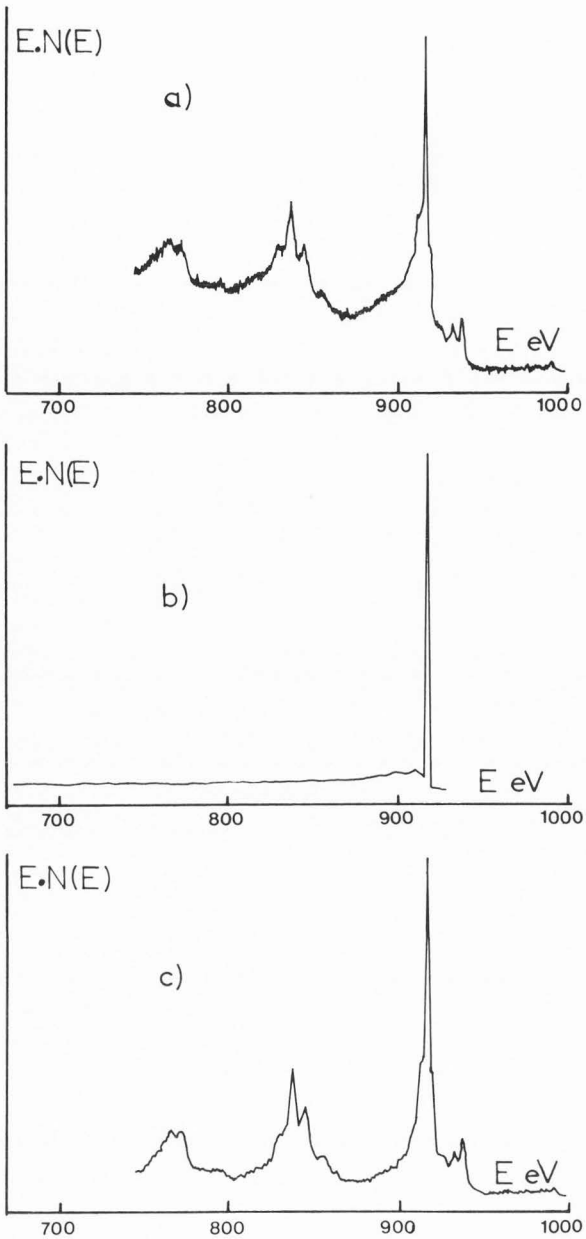

Fig. 3 Polycrystalline copper.
1024 channels, 0.25 eV per channel
a) LMM Auger spectrum
b) Backscattered electron energy spectrum
c) Deconvolution.

spectrometer axis. In figure 5, the surface is normal to the primary beam. In figure 6, two deconvoluted spectra are shown for comparison: the previous one (a) and another with the sample surface tilted about 45° away from the primary beam direction (b). In the latter case, the negative lobe increases in intensity. It was observed that the change was due to the back- scattered electron spectrum only.

Figure 7(a) shows spectra of the Te sample in a region that was slightly oxidised (as seen in

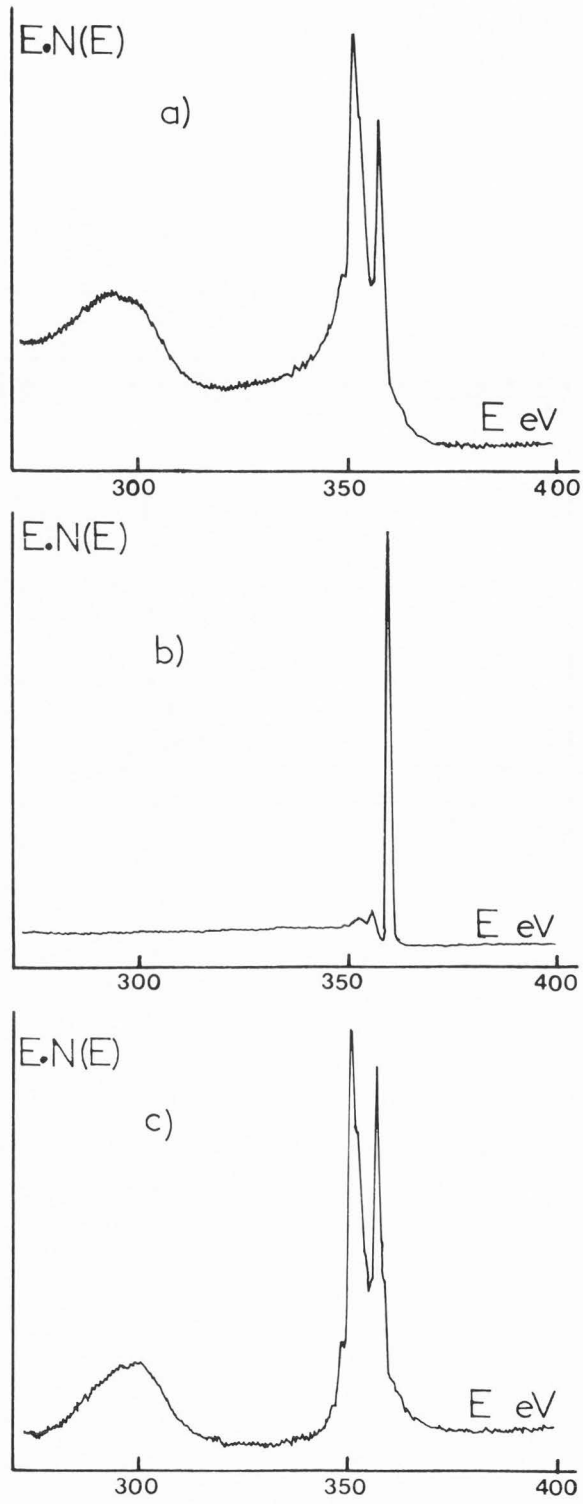

Fig. 4 Polycrystalline silver.
1024 channels, 0.125 eV per channel
a) MNN Auger spectrum
b) Backscattered electron energy spectrum
c) Deconvolution.

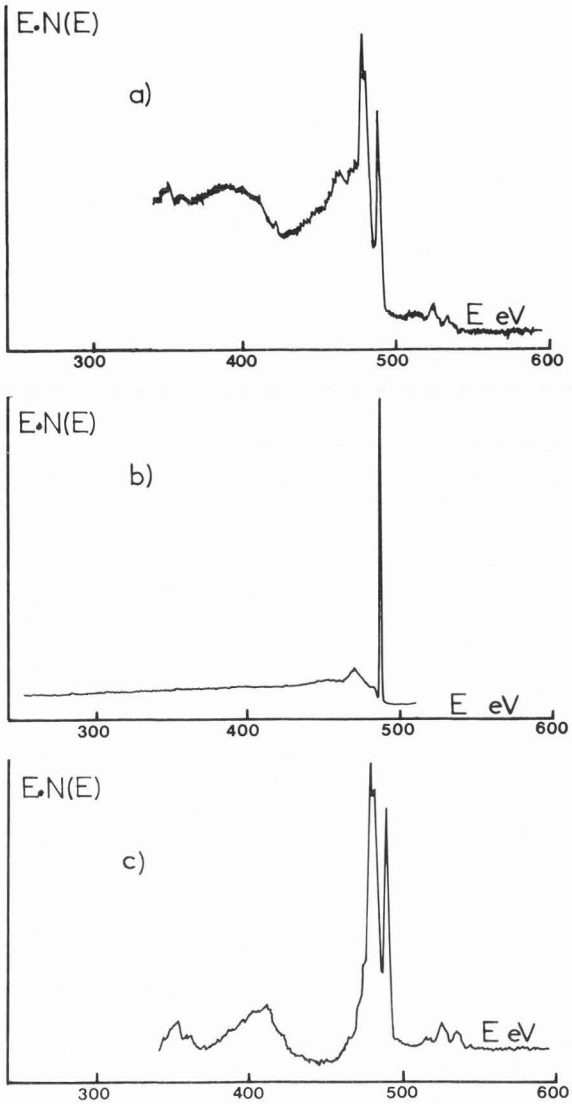

Fig. 5 Tellurium (1100) face, primary beam normal to surface.
1024 channels, 0.25 eV per channel
a) MNN Auger spectrum
b) Backscattered electron energy spectrum
c) Deconvolution.

peak labelled "O"), because that region of the sample was not exposed to the bombardment of argon ions. The corresponding deconvolution (figure 7(b)) does not show any negative lobe. In this case, the change is due again to the backscattered spectrum. Figure 8 shows for comparison enlarged plots of the inelastic tail for the clean and the oxidised Te surfaces.

Finally figure 9 presents a spectrum taken with the CMA spectrometer and its deconvolution. By comparison one can see that the deconvoluted spectrum has more or less the same resolution as its counterpart originated in the CHA which was operated at a relatively high energy resolution.

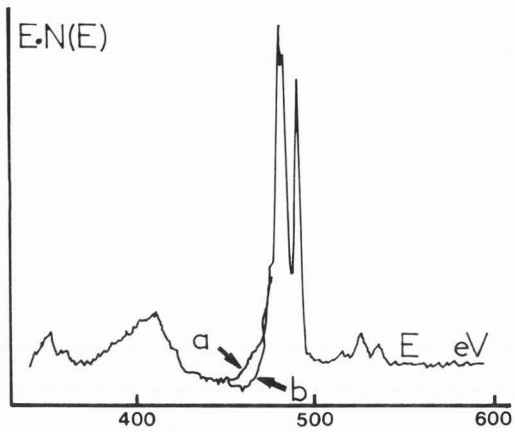

Fig. 6 Tellurium deconvoluted spectra.
a) Same as in Fig. 5-c
b) Sample tilted approx. 45°.

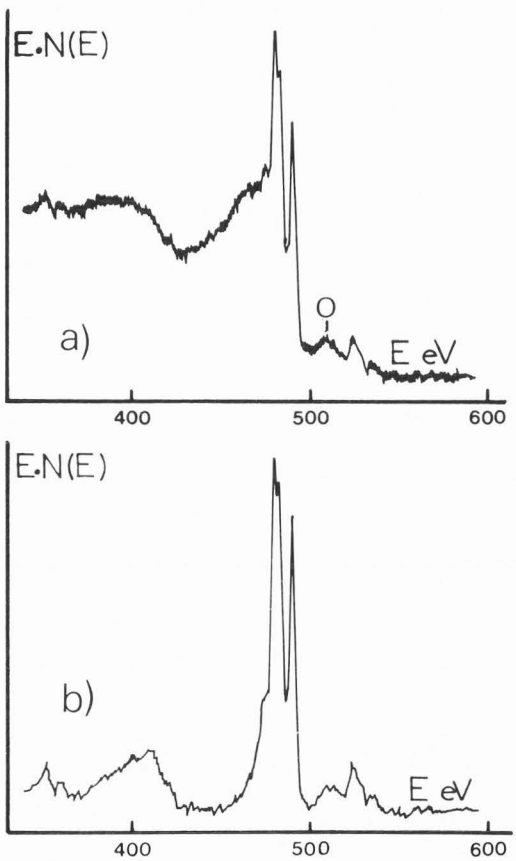

Fig. 7 Tellurium, slightly oxidized surface (a), and corresponding deconvoluted spectrum (b).
1024 channels, 0.25 eV per channel.

Discussion

We will consider two viewpoints: one is the use of deconvolution to simplify spectra by elimination of the inelastic losses. The other is the idea of using deconvolution to study loss

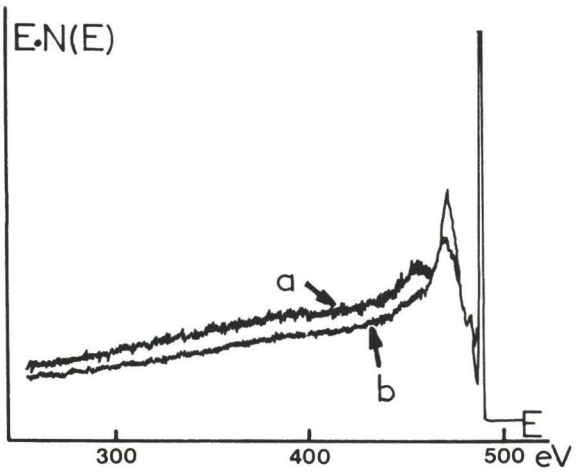

Fig. 8 Tellurium backscattered electron spectra.
a) Same as in Fig. 5-b
b) Corresponds to conditions of Fig. 7.

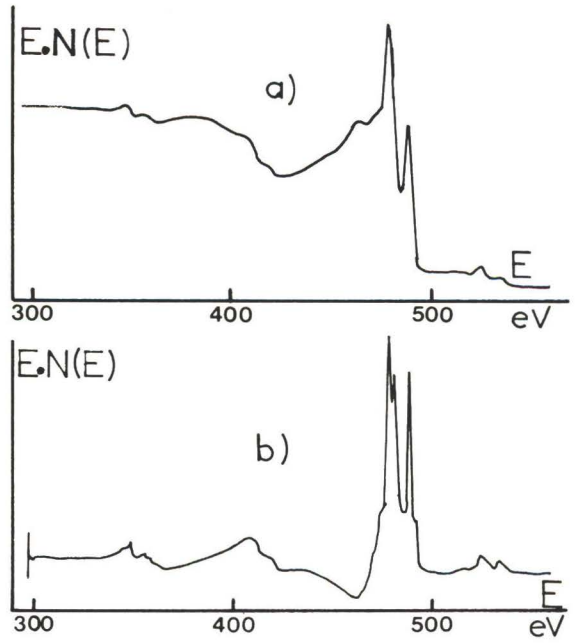

Fig. 9 Tellurium spectra taken with CMA spectrometer
a) MNN Auger spectrum
b) Deconvolution .

processes in electron spectroscopy (Auger, photoelectron and energy loss).

Now we will develop a continuum model for the loss effects. If we call λ_p the mean free path for volume plasmon generation, and s the distance the electron travels inside the solid, then the current I_n corresponding to the production of n plasmons in the electron path is given by a Poisson distribution, which is also valid for the no-loss line (n = 0):

$$I_n = \frac{1}{n!} \left(\frac{S}{\lambda_p}\right)^n \exp\left(-s/\lambda_p\right) \qquad (2)$$

This expression can be used when all electrons travel the same distance s in the solid. This condition is met in experiments done on thin films in a transmission geometry (Spence and Spargo, 1971). In our case, however, the path length, s, is not a constant, but a variable with a distribution T(s) (normalised). Thus we obtain:

$$I_n = \frac{1}{n!} \int_0^\infty \left(\frac{S}{\lambda_p}\right)^n \exp\left(-s/\lambda_p\right) T(s)\, ds \qquad (3)$$

We can see in equation (3) that the intensity of the plasmons depends strongly on the shape of the distribution T(s). The geometrical parameters of the experiment: position of the electron source, orientation of the analyser axis, angular acceptance of the analyser, have a strong influence on T(s). Therefore, the elastic peak and the Auger or photoelectron peaks exhibit different tails due to the difference in T(s). If one considers an Auger or photoelectron experiment with the electron sources distributed homogeneously in the sample, one can use:

$$T(s) = \frac{1}{\lambda_o} \exp\left(-s/\lambda_o\right) \qquad (4)$$

where λ_o is the mean free path for excitations other than plasmons (e.g. ionisations). Introducing this particular expression for T(s) and evaluating the integral in (3) we get:

$$I_n = \frac{\lambda_p}{(\lambda_o + \lambda_p)} \frac{\lambda_o^n}{(\lambda_o + \lambda_p)^n} \qquad (5)$$

which is essentially the result of the model used by Pardee et al. (1975) to study plasmon losses in photoemission.

On the other hand, if one considers the backscattered electron spectrum, the source of electrons is located outside the solid and elastic scattering must be effective to direct the electrons towards the analyser. This is due to the fact that loss transitions have a differential cross section with a very narrow angular distribution, while elastic processes have a broader angular distribution.

It is easy to understand that if in a backscattering measurement the analyser is in the specular direction, the distribution T(s) will give more weight to small values of s, resulting in small plasmon losses, probably smaller than (5). Diffraction of the primary beam also produces changes both in the elastic and plasmon peaks (Le Gressus et al., 1983). The anisotropy of Auger emission due to diffraction effects (Baudoing et al., 1983; Koshikawa et al., 1981) must be produced by drastic changes in T(s) when the geometric parameters of the measurement are varied.

Even in a situation where diffraction effects could be neglected, the distribution (4) may not be valid due to elastic scattering. Ganachaud and

Cailler (1979), and Jablonski and Ebel (1984) among others have shown by means of Monte-Carlo calculations that elastic scattering reduces the effective escape depth of electrons, which is a very important factor in the quantification of Auger or photoelectron spectroscopy. Tougaard and Sigmund (1982) have studied the problem theoretically, obtaining analytical expressions in some limiting cases. They consider a diffusion model for all elastic collisions, use the Boltzmann transport equation and define an elastic transport mean free path λ_1 which is normally smaller than the inelastic mean free path $\lambda_{in} = \lambda_o\lambda_p/(\lambda_o+\lambda_p)$. Equation (35) of Tougaard and Sigmund's paper can be written according to our notation as:

$$Q \sim \left(\frac{3\ x^2}{4\pi^3\ \lambda_1\ s^3}\right)^{\frac{1}{2}} \exp\left(-\frac{3\ x^2}{4\lambda_1\ s}\right) \cos\theta \qquad (6)$$

which is the path distribution for electrons coming out of an isotropic point source located inside the solid at a distance x from the surface, and θ is the angle of emergence of the electrons away from the normal. This expression is valid for $s > 2\lambda_1$. For smaller values of s, a diffusion process is not a good representation of the real motion of the electrons. If the point sources are homogeneously distributed inside the solid, we can integrate for all x, arriving to equation (39) of Tougaard and Sigmund's paper:

$$\int Q\ dx = \left(\frac{\lambda_1}{3\pi^3\ s}\right)^{\frac{1}{2}} \cos\theta \quad s > 2\ \lambda_1 \qquad (7)$$

In order to get the path distribution T(s) within this model we need the mean free path λ_o for losses excluding plasmons and to normalize:

$$T(s) = \frac{1}{\sqrt{\pi}\ \lambda_o}\ s^{-\frac{1}{2}} \exp(-s/\lambda_o) \qquad (8)$$

Introducing this path distribution in eq. (3), we get:

$$I_n = \frac{1}{n!\ \sqrt{\pi}} \left(\frac{\lambda_{in}}{\lambda_p}\right)^n \left(\frac{\lambda_{in}}{\lambda_o}\right)^{\frac{1}{2}} \Gamma\left(n + \frac{1}{2}\right) \qquad (9)$$

In particular, for n = 0, and n = 1 we get:

$$\frac{I_1}{I_o} = \frac{1}{2}\left(\frac{\lambda_{in}}{\lambda_p}\right) = \frac{1}{2}\left(\frac{\lambda_o}{\lambda_o + \lambda_p}\right) \qquad (10)$$

This result differs in a factor $\frac{1}{2}$ from the previous model which did not consider diffusion through elastic scattering (eq. 5). Higher order plasmons have different expressions in each model. Again from eq. (9) we get:

$$\frac{I_n}{I_{n-1}} = \left(\frac{\lambda_o}{\lambda_o + \lambda_p}\right)\left(1 - \frac{1}{2n}\right) \qquad (11)$$

whereas the no-elastic scattering model did not have the second factor at the right hand side of (11). The difference is more important for low n.

The applicability of the diffusion model depends on the ratio between elastic and inelastic mean free paths. It is obviously a good model if the ratio is much smaller than one. In real materials the ratio is certainly less than one, but may not satisfy this criterion. If we take for example the case of aluminium at 1 keV electron energy, the elastic mean free path is 14 Å (Ganachaud, 1977) and the inelastic mean free path is 32.4 Å. For elements with higher atomic numbers, the elastic scattering cross section is larger and we would expect a closer approach to the diffusion model. The two models presented are limiting cases, and the real materials may give results between them.

So far we have considered an isotropic source of electrons distributed homogeneously in the solid to describe Auger or photoelectron scattering processes. The situation for the backscattered electron spectrum is completely different. Here the source is not isotropic and is not located within the solid. There are many studies of electron beam penetration and its effects using Monte Carlo methods in the field of electron microprobe analysis (Bishop, 1967; Samoto and Shimizu, 1983) or secondary electron emission (Ganachaud and Cailler, 1979). However, to our knowledge nobody has considered the related problem of finding the plasmon intensities. In the absence of a well developed theory or calculation, we present here an estimate based on the previous models. In the diffusion case, let us take a point emission source at distance x from the surface. We shall assume that x is of the order of λ_1 so as to randomize the electron angular distribution for such a source. The path distribution, once normalized is:

$$T(s) = \frac{x}{2}\left(\frac{3}{\pi\ \lambda_1}\right)^{\frac{1}{2}} \exp\left(\frac{x}{\sqrt{\lambda_1\lambda_o/3}}\right) s^{-3/2} \exp\left(\frac{-3x^2}{4\ \lambda_1\ s}\right) \cdot \exp(-s/\lambda_o) \qquad (12)$$

Introducing this expression for T(s) in (3) we get:

$$I_n = \frac{x}{2}\left(\frac{3}{\pi\ \lambda_1}\right)^{\frac{1}{2}} \exp\left(\frac{x}{\sqrt{\lambda_1\lambda_o/3}}\right) \frac{1}{n!} \cdot \int_0^\infty \left(\frac{s}{\lambda_p}\right)^n s^{-3/2} \exp\left(-\frac{s}{\lambda_{in}}\right) \exp\left(-\frac{3x^2}{4\ \lambda_1\ s}\right) ds \qquad (13)$$

Finally, we obtain for the ratio of the first plasmon to the no-loss peak (n = 1 and n = 0):

$$\frac{I_1}{I_o} = \frac{1}{2}\frac{\lambda_{in}}{\lambda_p}\frac{x}{\sqrt{\lambda_1\ \lambda_{in}/3}} = \frac{1}{2}\left(\frac{\lambda_o}{\lambda_o + \lambda_p}\right)\frac{x}{\sqrt{\lambda_1\ \lambda_{in}/3}} \qquad (14)$$

The latter value does not pretend to be the result of an exact calculation since x does not have a definite meaning. It is something like an effective distance from the surface where an isotropic source of electrons is located. The primary beam is supposed to penetrate the solid without interactions up to a distance x, where elastic collisions randomize the electron velocities. Let us call $x = \xi\lambda_1$ where ξ is of the order of unity. Then:

$$\frac{I_1}{I_o} = \frac{1}{2}\left(\frac{\lambda_o}{\lambda_o + \lambda_p}\right) \xi \sqrt{3\lambda_1/\lambda_{in}} \qquad (15)$$

From this result it is inferred that, in general, the relative plasmon peak intensity near the elastic peak will be different to that of Auger or photoelectron emission, due to elastic scattering. This is not the case in the no-elastic scattering model, since the primary beam is just attenuated in depth because of inelastic scattering, resulting in the same value for backscattering and for Auger emission.

Our conclusion agrees qualitatively with the simplified model of Matthew and Underhill (1978), where they considered elastic backscattering only in the backward direction.

From the point of view of deconvolution performance, the no-elastic scattering model predicts complete plasmon cancellation, while the diffusion elastic scattering model predicts incomplete cancellation or over-cancellation depending on the values of ξ and λ_1/λ_o.

The model presented does not take into account diffraction effects, which are known to be important since the plasmon and the no-loss peaks change in intensity in a different manner near Bragg conditions (Le Gressus et al., 1983).

Another important effect is surface plasmon production. Matthew and Underhill (1978) pointed out that Auger electrons cross the surface only once, whereas backscattered electrons cross it twice. Thus deconvolution will over-compensate for surface plasmon peaks. This has been confirmed by Célier (private communication). By varying the incidence and take-off angles, she has been able to obtain different surface plasmon intensities in aluminium single-crystal samples. At angles far away from normal incidence and take-off, the surface plasmon peak is big enough to yield a negative peak upon deconvolution.

Silver is a special case because volume and surface plasmon peaks are very close in energy, as inferred from optical measurements which show a very steep rise of ε near 3.8 eV (Ehrenreich and Philipp, 1962). The peaks are so close that they are usually not resolved in energy loss spectra. The broad negative dip in our deconvoluted silver spectrum (figure 4) may be partially explained by this effect.

In the case of tellurium there is no overlap between the surface and volume plasmons, so that the explanation for the negative dip must be found elsewhere. It is noteworthy that this effect is not exceptional. Koenig and Grant (1984) have reported a similar situation in CdSe spectra. In the tellurium case, an important property can be invoked to explain the negative dip: the anisotropy of elastic scattering. Bammes et al. (1972) have measured energy loss spectra in electron transmission through tellurium thin films, finding that the relative intensity of the plasmon peak was bigger when the scattering was in a direction perpendicular to the z-axis. Bammes (1973) attributed this difference to the anisotropy of elastic scattering. In our experiment, it is clear that the backscattered spectrum is more influenced by elastic scattering than the Auger spectrum, since in the former the total scattering angle is greater (near 180°).

There is an interesting case in which all the above considerations about elastic scattering do not apply: if there is one monolayer of adsorbed atoms or molecules, the escape distance is just one monolayer for those Auger electrons generated by the adsorbed species. On the other hand, electrons coming from the substrate may have a longer escape distance, which is determined by the cross sections for elastic scattering, plasmon production, core and band electron excitation, etc. Also the backscattered electrons in the elastic peak spectrum may have an average path length of several atomic distances. From this consideration it follows that deconvolution with the elastic peak spectrum as a unit response function will over-compensate for plasmon peaks in those Auger spectra of monolayer adsorbed species. Such a situation was recognised by Campbell et al. (1980) and Kelber et al. (1982). Instead of using the elastic peak spectrum, they measured a photoelectron spectrum around a 1s peak of nitrogen or oxygen. In these experiments, the same emission geometry is achieved for the Auger spectrum and for the unit response spectrum. It must be remembered, however, that the kinetic energies are not the same. For the unit response function, photoelectrons are excited by Mg K_α radiation, resulting in a kinetic energy of about 850 eV, whereas KVV electrons have about 380 eV energy (N) or 510 eV (O). Thus this procedure may not be generally applicable. For example, Flodstrom et al. (1977) recorded photoelectron spectra of aluminium and silicon using tunable synchrotron radiation and demonstrated the dependence of volume and surface plasmon intensity on the photoelectron kinetic energy. It has been proposed (Ramaker et al., 1979) to use a tunable radiation source to produce a unit response function from photoelectrons of about the same kinetic energy as the Auger electrons. Such a proposal will certainly ensure the same emission geometry and the same scattering parameters, but the experimental requirements are stringent due to the limited availability of tuned radiation sources.

The deconvolution of aluminium spectra shows clearly incomplete plasmon cancellation, especially for the first volume plasmon. This can be explained by the intrinsic process of plasmon generation during the Auger process. The subject has been studied theoretically (Chang and Langreth, 1973; Penn, 1977 and Bose et al., 1983), and measurements have been made to demonstrate its occurrence (Pardee et al., 1975; Van Attekum and Trooster, 1978; Steiner et al., 1978; Norman and Woodruff, 1979). However, the experimental verification is not conclusive since the results obtained depend on the type of least-squares curve fitting employed. Pardee et al. (1975) adjusted a simple Lorentzian to each loss peak, in order to obtain the area assigned to plasmons of different order. The result was that the intensities followed a geometric progression as in equation (5) so that intrinsic plasmon production was judged

negligible. Van Attekum and Trooster (1978) realised that the loss peaks were asymmetrical, and adjusted two half-Lorentzians to each peak, thereby attributing a 25% contribution to intrinsic processes. This discrepancy is due to the sensitivity of the least-squares curve fitting methods to the number of parameters employed. On the other hand, in these papers there is the implicit assumption that no elastic scattering is involved. As we have seen earlier, elastic scattering not only decreases the escape distance, but also changes the relative intensity of plasmons, so that different intrinsic contributions could be obtained from the same experimental data if elastic scattering is taken into account. After these considerations, one can see that deconvolution calculations may be very useful for studying intrinsic processes, since one can expect a reasonable cancellation of the extrinsic losses, leaving only the intrinsic ones. In our aluminium spectra, the residual first plasmon after deconvolution is so great that it could never be attributed solely to differences in emission geometry. Also, the residual second plasmon is very small, in good agreement with the idea of intrinsic plasmon production. The great advantage of deconvolution is that there is not any assumption regarding the shape of the electron spectra or the loss spectra (no adjustable parameters of any kind). On the other hand, the theoretical calculations mentioned earlier involve several approximations, so that their results have only a qualitative value. For this reason we believe that the residual first plasmon from aluminium deconvoluted spectra is the most realistic evidence of intrinsic plasmon production in KLL transitions.

Finally, one word about resolution enhancement. If the aim of a deconvolution is to enhance resolution, the spectrum must show a good signal to noise ratio since it is generally accepted that the procedure enhances noise (Jones and Misell, 1970). Our results confirm this situation. The CMA has a nominal resolution of 0.3% which may smooth out some Auger features. The Te spectrum shown in Figure 9 was taken with the CMA in the derivative mode and then integrated, and the noise is so small that it is not visible in the graph. Deconvolution yielded improved resolution, which is evident by comparison with other Te spectra taken with the CHA at higher resolution (figures 5, 6 and 7). The latter did not yield improved resolution through deconvolution because the raw signal-to-noise ratio was not good enough, and the filter window was chosen to limit the noise; in this way, the filter counteracted any improvement in resolution that could have been obtained by means of deconvolution.

Conclusions

The results presented on deconvolutions of Al, Ni, Cu, Ag and Te spectra have demonstrated the usefulness of the method to simplify spectra and sometimes to increase resolution. We believe that the modified algorithm employed is a significant step towards the credibility of the method because it avoids Gibbs oscillations without sacrificing the ability to improve resolution. The discussion was centred around the problem of achieving an exact cancellation of the loss features. It was shown on the basis of a simple diffusion model with elastic scattering that this was not the case in general. At this time it seems that Monte Carlo calculations could be very helpful in establishing a correction to the backscattered spectrum so that it could be used in a deconvolution rendering exact cancellation. Diffraction effects would require additional care. Deconvolution does not remove intrinsic losses (as in Al), suggesting the method can be used to study them.

Acknowledgements

We are grateful to Dr. J.P. Duraud and to Dr. J.A.D. Matthew for very fruitful conversations.

References

Bammes P (1973). Anisotropy of Elastic Electron Scattering in Energy Loss Experiments on Te. Phys. Stat. Sol. (b) 57, K19-K20.

Bammes P, Klucker R, Koch EE, Tuomi T (1972). Dielectric Constants of Trigonal Se and Te between 3 and 30 eV. Phys. Stat. Sol. (b) 49, 561-570.

Baro AM, Tagle JA (1978). The $L_{2,3}VV$ Auger Spectrum of Mg. J. Phys. F: Metal Phys. 8, 563-569.

Baudoing R, Gaubert C, Blanc E, Aberdam D, Gauthier Y (1984). Anisotropic Emission in Electron Spectroscopy. Scanning Electron Microsc. 1984; I: 87-102.

Bishop HE (1967). Electron Scattering in Thick Targets. Brit. J. Appl. Phys. 18, 703-715.

Bishop HE, Chornik B, Le Gressus C, Le Moel A (1984). Crystalline Effects in Auger Electron Spectroscopy. Surf. and Interf. Anal. 6, 116-128.

Bose SM, Prutzer S, Longe P (1983). Plasmon Satellites in the X-ray Photoemission Spectra of Metals and Adsorbates. Phys. Rev. B27, 5992-5999.

Campbell ChT, Rogers JW Jr, Hance RL, White JM (1980). Auger Spectra of Ammonia on Al and Oxidised Al. Chem. Phys. Lett. 69, 430-434.

Carley AF, Joyner RW (1979). The Application of Deconvolution Methods in Electron Spectroscopy - A Review. J. Electron Spectros. 16, 1-23.

Chang JJ, Langreth DC (1973). Deep-hole Excitations in Solids. II: Plasmon and Surface Effects in X-ray Photoemission. Phys. Rev. B8, 4638-4654.

Ehrenreich H, Philipp HR (1962). Optical Properties of Silver and Copper. Phys. Rev. 128, 1622-1629.

Flodstrom SA, Bachrach RZ, Bauer RS, McMenamin JC, Hagstrom SBM (1977). Investigation of Plasmon Sidebands by Synchrotron Radiation Tuning of Electron Escape Depths. J. Vac. Sci. Technol. 14, 303-306.

Ganachaud JP (1977). Contribution à l'étude théorique de l'émission électronique secondaire des métaux. Thesis, University of Nantes, France.

Ganachaud JP, Cailler M (1979). A Monte Carlo Calculation of the Secondary Electron Emission of Normal Methods. Surf. Sci. 83, 498-530.

Harris FJ (1978). On the Use of Windows for Harmonic Analysis with the Discrete Fourier Transform. Proc. IEEE 66, 51-83.

Helms HD (1967). Fast Fourier Transform Method of Computing Difference Equations and Simulating Filters. IEEE Tans. on Audio and Electroacust. AU-15, 85-90.

Houston JE (1975). Valence-band Structure in the Auger Spectrum of Al. J. Vac. Sci. Technol. 12, 255-259.

Hutson FL, Ramaker DE, Dunlap BI (1982). Interpretation of the Nitrogen KVV Auger Line Shape from Alkali Metal Nitrates. J. Chem. Phys. 76, 2181-2190.

Jablonski A, Ebel H (1984). Effects of Elastic Photoelectron Collisions in Quantitative XPS. Surf. Interf. Anal. 6, 2-28.

Jansson PA (1970). Method for Determining the Response Function of a High-Resolution Infrared Spectrometer. J. Opt. Soc. Amer. 60, 184.

Jennison DR (1980). Auger Lineshape Analysis of Molecules and Solids. J. Vac. Sci. Technol. 17, 172-175.

Jones AF, Misell DL (1970). The Problem of Error in Deconvolution. J. Phys. A 3, 462-472.

Kelber JA, Rye RR, Nelson GC, Houston JE (1982). Auger Spectroscopy of Polyethylene and Poly(ethylene oxide). Surf. Sci. 116, 148-162.

Koenig MF, Grant JT (1984). Deconvolution in X-ray Photoelectron Spectroscopy. J. Electron Spectros. Rel. Phen. 33, 9-22.

Koshikawa T, Von dem Hagen T, Bauer E (1981). Angle-resolved investigation of Auger electrons from Cu and Au adsorbed on W(110). Surf. Sci. 109, 301-310.

Le Gressus C, Duraud JP, Massignon D, Lee-Deacon O (1983). Electron Channelling Effect on Secondary Electron Image Contrast. Scanning Electron Microsc. 1983; II: 537-542.

Madden HH (1983). Auger Lineshape Analysis. Surf. Sci. 126, 80-100.

Madden HH, Houston JE (1976). Correction of Distortions in Spectral Line Profiles: Applications to Electron Spectroscopies. J. Appl. Phys. 47, 3071-3082.

Madden HH, Zehner DM, Noonan JR (1978). $L_{2,3}VV$ and MVV Auger Spectra of Cu. Phys. Rev. B17, 3074-3088.

Matthew JAD, Underhill PR (1978). The Use of Electron Loss Data as Unit Impulse Response Function in Deconvolution of Electron Spectra. J. Electron Spectros. Rel. Phen. 14, 371-377.

Mularie WM, Peria WT (1971). Deconvolution Techniques in Auger Electron Spectroscopy. Surf. Sci. 26, 125-141.

Norman D, Woodruff DP (1979). Plasmon Losses Structure in Synchrotron Radiation Photoemission from Mg Films. Surf. Sci. 79, 76-92.

Pardee WJ, Mahan GD, Eastman DE, Pollak RA, Ley L, McFeely FR, Kowalczyk SP, Shirley DA (1975). Analysis of Surface - and Bulk Plasmon Contributions to X-ray Photoemission Spectra. Phys. Rev. B11, 3614-3616.

Penn DR (1977). Theory of the Electron Energy-loss Spectrum in Core-level X-ray Photoemission From Solids. Phys. Rev. Lett. 38, 1429-1432.

Ramaker DE, Murday JS, Turner NH (1979). Extracting Auger Lineshapes from Experimental Data. J. Electron Spectr. Rel. Phen. 17, 45-65.

Samoto N, Shimizu R (1983). Theoretical Study of the Ultimate Resolution in Electron Beam Lithography by Monte-Carlo Simulation, Including Secondary Electron Generation: Energy Dissipation Profile in Polymethylmethacrylate. J. Appl. Phys. 54, 3855-3859.

Spence JCH, Spargo AEC (1971). Observation of Double Plasmon Excitation in Al. Phys. Rev. Lett. 26, 895-897.

Steiner P, Hochst H, Hufner S (1978). XPS Investigation of Simple Metals. I: Core Level Spectra. Z. Phys. B30, 129-143.

Tagle JA, Martinez-Saez V, Rojo JM, Salmeron M (1978). Obtaining Density of States Information from Self-Deconvolution of Auger Band-type Spectra. Surf. Sci. 77, 77-93.

Tougaard S, Sigmund P (1982). Influence of Elastic and Inelastic Scattering on Energy Spectra Emitted from Solids. Phys. Rev. B25, 4452-4466.

Van Attekum PHThM, Trooster JM (1978). Bulk and Surface Plasmon Loss Intensities in Photoelectron, Auger and Electron Energy-loss Spectra of Al. Metal. Phys. Rev.B18, 3872-3883.

Wertheim GK (1975). Deconvolution and Smoothing: Applications in ESCA. J. Electron Spectros. Rel. Phen. 6, 239-251.

Discussion with Reviewers

D.C. Peacock: Could you clarify your conclusions as to the applicability of the technique to the simplification of spectra for quantitative AES? Do you think that the residual rising background (Fig. 3) in your "Results" section, which may prove to be a source of error in integration of peak areas,arises because initial subtraction of a linear background is inadequate? Would the subtraction of a more physical background obviate this?

Authors: Quantitative AES schemes must deal with the problem of background subtraction. It is well known that at low energies a linear background is not adequate because of the presence of the secondary electron tail. Higher order backgrounds involve the calculation of a number of parameters by curve fitting methods and/or additional physical assumptions. The background can be easily identified at the high energy side of a group of Auger peaks if there are no Auger peaks at higher energies. What we have done is to extrapolate the background from the high energy side of the spectrum. By doing that we can subtract a substantial amount of the real background. The residual was left as part of the spectrum (for example in Fig. 3). We agree that it should be eliminated if a quantitative AES calculation is undertaken, but this was not our concern in this work.

M.F. Koenig: The data obtained in the CMA were "numerically integrated" to obtain th E.N(E) spectra. If standard integration algorithms were employed which set the right side of the spectrum to zero before integrating, a linear background was subtracted from your data. From the description of your deconvolution algorithm, it sounds like you also subtracted a linear background from the data obtained with a hemispherical analyser. Having already subtracted some of the background from the data peaks, is it really surprising that the spectra after deconvolution with the backscattered electron spectra exhibit negative-going tails?
Authors: Assuming that the background is a smooth function of energy (neglecting ionisation features) we would expect either a straight line or else a curve with non-negative second derivative for the background intensity with respect to energy. This is so because of the secondary electron tail and the primary beam tail due to multiple scattering. With such a background, if one fits a straight line to a portion of the background at the right side, and then subtracts the straight line from the spectrum, one would always obtain a zero or positive residual background at the left side upon deconvolution. In some cases we have obtained negative going peaks, and we attribute these results to differences in scattering processes that produce the inelastic tail of the Auger spectrum and of the primary beam spectrum (as explained in the text).

M.F. Koenig: Most of the data were collected in the constant retard ratio mode. Since you have performed the deconvolutions over several hundred electron volts, the pass energy and hence the analyser resolution is varying a significant amount (i.e., over 0.05 eV). Therefore, the backscattered electron spectrum taken at the high kinetic energy end of the data is no longer a valid representation of the losses or analyser resolution function at the low kinetic energy end of the data. How do you deal with this discrepancy? Are several backscattered electron spectra taken and used over only small intervals of the data, or does the deconvolution algorithm automatically adjust the width of the elastically backscattered peak?

D.C. Peacock: Was a single backscattered electron spectrum used to approximate h(E) over the entire energy range of each Auger spectrum? Burrell et al. (Appl. Surf. Sci. 17 (1983) 53-69) found it necessary in some cases to use several backscattered spectra over similar energy ranges to allow for the energy dependence of the scattering function (see, for example, Fig. 4 of Burrell et al. for the difference in Ti loss function for primary energies in the range 400 to 470 eV). Would not the energy dependence of the spectrometer window ΔE in the present work make this even more necessary?
T.J. Shaffner: Is not the deconvolution technique you describe optimum only for the particular energy used to obtain the backscattered electron spectrum?
Authors: The widest spectrum was that of Ni, with a 250 eV span, and the narrowest spectrum was that of Al, with a 130 eV span. In all cases the energy of the primary beam for the unit response spectrum was close to the energy of the most interesting features of the Auger spectrum. It is true that the analyser resolution varies through the spectrum, but this variation is not always relevant. For the Al spectrum, it is indeed negligible because resolution changes from 1.6 to 1.7 eV (corresponding to 1300 and 1400 eV respectively). For the Te spectrum, resolution goes from 0.47 to 0.59 eV (corresponding to 390 and 490 eV), which is not a negligible change, but the Auger peaks at low energy are very broad so that they are not deformed anyway. All other spectra are intermediate situations between Al and Te. Therefore it was judged not necessary to undertake a correction scheme, which would probably involve a combination of a number of backscattered electron spectra taken at different primary beam energies.

D.C. Peacock: Burrell et al (op. cit.) claim that their sequential approximation to deconvolution is a useful and accurate alternative to Van Cittert deconvolution techniques for quantitative AES. It is certainly quicker than the method described in the present work. Please would you comment on this and point out any advantages that your method has over the sequential method.
Authors: Burrell et al's method is not quicker than ours because it cannot be adapted to FFT calculations. If n is the number of points in the spectrum, then n^2 multiplications are required in their method. By comparison, each convolution using FFT requires of the order of n.log(n) multiplications. Burrell et al's method essentially replaces the unit response function by a Dirac delta plus a tail (which is an approximation), and their calculation is equivalent to one of our deconvolutions with this modified response function. Therefore, this method cannot improve resolution, and only eliminates the tail of electron spectra. Our deconvolutions eliminate the tail and also have the potential capability of improving resolution if the raw signal-to-noise ratio is good enough.

T.J. Shaffner: You mention that the signal-to-noise ratio in the CMA spectrum is very good relative to the CHA spectrum. This is to be expected from the fact that integration of the N'(E) spectrum again imposes a low pass filter

(cf., Pocker et al, J. Vac. Sci. Technol. 13, 1976, 507-511). Therefore, is not your deconvolution in Fig. 9 simply recouping the resolution lost by imposition of a low-pass smoothing function in the Fourier space?

Authors: The low pass filter inserted at the output of the lock-in amplifier does not limit resolution provided that the sweep speed is low enough. Resolution is only determined by the analyser geometry and the modulation amplitude. In our case, the CMA resolution was 0.3%, and the modulation was 0.5 V p.t.p. which had a negligible effect. On the other hand, the fact that the derivative mode enhances sharp features over the background, has led some authors to state that a low pass filter is imposed under numerical integration. This is not true. Information is not lost nor retrieved with such a calculation. It is just presented in a different way. The main reason for the good signal-to-noise ratio in Fig. 9 is that the primary beam current of about 5 μA is much higher than the current of 1 nA in the other cases. The CMA gives 0.3% resolution, which is not very good, but the good signal-to-noise ratio allows resolution enhancement through deconvolution. In all other cases, resolution was about 0.12% but noise was indeed visible and prevented any improvement by means of deconvolution.

T.J. Shaffner: If you change the primary beam energy for the backscattered spectrum in Fig. 1 for example, to 1300 eV, do you observe significant changes in the energy loss peak structure and shape?

Authors: There were no changes in the relative amplitude of the tail when the primary beam energy was varied within the range of the corresponding Auger spectra. We did not observe any effect related to diffraction of the primary beam in the polycrystalline samples. For the Al single crystal, relative intensity of the plasmon peaks remained constant near diffraction conditions (as explained in the text).